JACS Au
AN OPEN ACCESS JOURNAL OF THE AMERICAN CHEMICAL SOCIETY

Open Access
This article is licensed under CC-BY 4.0

pubs.acs.org/jacsau
Article

Visualizing Actin Packing and the Effects of Actin Attachment on Lipid Membrane Viscosity Using Molecular Rotors

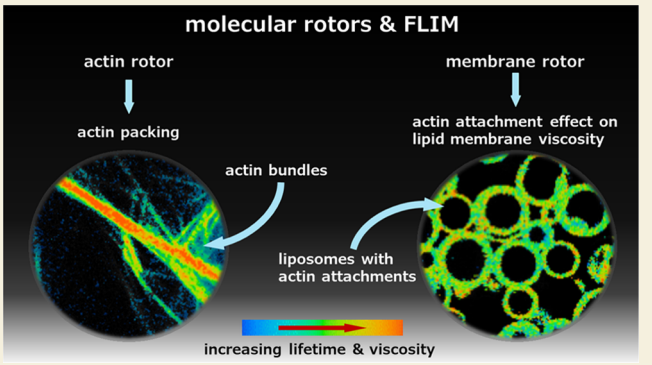
Ion A. Ioannou, Nickolas J. Brooks,* Marina K. Kuimova,* and Yuval Elani*

Cite This: JACS Au 2024, 4, 2041−2049

Read Online

ACCESS | Metrics & More | Article Recommendations | Supporting Information

ABSTRACT: The actin cytoskeleton and its elaborate interplay with the plasma membrane participate in and control numerous biological processes in eukaryotic cells. Malfunction of actin networks and changes in their dynamics are related to various diseases, from actin myopathies to uncontrolled cell growth and tumorigenesis. Importantly, the biophysical and mechanical properties of actin and its assemblies are deeply intertwined with the biological functions of the cytoskeleton. Novel tools to study actin and its associated biophysical features are, therefore, of prime importance. Here we develop a new approach which exploits fluorescence lifetime imaging microscopy (FLIM) and environmentally sensitive fluorophores termed molecular rotors, acting as quantitative microviscosity sensors, to monitor dynamic viscoelastic properties of both actin structures and lipid membranes. In order to reproduce a minimal actin cortex in synthetic cell models, we encapsulated and attached actin networks to the lipid bilayer of giant unilamellar vesicles (GUVs). Using a cyanine-based molecular rotor, $DiSC_2(3)$, we show that different types of actin bundles are characterized by distinct packing, which can be spatially resolved using FLIM. Similarly, we show that a lipid bilayer-localized molecular rotor can monitor the effects of attaching cross-linked actin networks to the lipid membrane, revealing an increase in membrane viscosity upon actin attachment. Our approach bypasses constraints associated with existing methods for actin imaging, many of which lack the capability for direct visualization of biophysical properties. It can therefore contribute to a deeper understanding of the role that actin plays in fundamental biological processes and help elucidate the underlying biophysics of actin-related diseases.



KEYWORDS: *actin, vesicles, fluorescence lifetime imaging microscopy (FLIM), membrane packing, molecular rotors, synthetic cell models, membrane biophysics*

Downloaded via IMPERIAL COLLEGE LONDON on July 16, 2024 at 15:20:14 (UTC).
See https://pubs.acs.org/sharingguidelines for options on how to legitimately share published articles.

INTRODUCTION

Actin, being one of the most abundant proteins in eukaryotic cells, has a critical role in a host of cellular processes such as cell movement, division, and structural support.[1] Actin polymerizes into filaments that constitute the core component of the cytoskeleton, and their function is regulated by actin-binding proteins (ABPs) and various signaling pathways.[2−4] Dysregulation of actin and ABPs can have extensive implications on cellular function and has been reported to contribute to a wide range of diseases. Among them, actin myopathies can affect the normal function of skeletal muscles and the heart,[5,6] and abnormalities of the actin cytoskeleton are also associated with cancer development and metastasis. For example, it is well established that overexpression of fascin, an actin-bundling protein, has a crucial role in breast cancer development and can give rise to cancer cell migration, invasion, and metastatic colonization.[7,8]

To date, the most common techniques used to visualize the actin cytoskeleton and ABPs are fluorescence and electron microscopies.[9,10] The latter can achieve nanometer-range resolution but has limitations when applied to live and wet biological samples due to the high vacuum conditions required in the specimen chamber.[11] On the contrary, fluorescence microscopy is extensively applied to live cells, and the recent development of super-resolution technologies has enabled researchers to overcome the light diffraction limit and achieve optical resolution down to ∼1 nm.[12−15] The development of numerous fluorescent probes and their coupling to actin-binding compounds (*e.g.*, phalloidin) and antibodies have also permitted simultaneous visualization of multiple targets with high specificity.[16] Although both electron and light microscopies constitute powerful tools in cytoskeletal studies, current applications are focused on providing morphological and

Received: March 14, 2024
Revised: April 10, 2024
Accepted: April 11, 2024
Published: April 30, 2024



© 2024 The Authors. Published by American Chemical Society

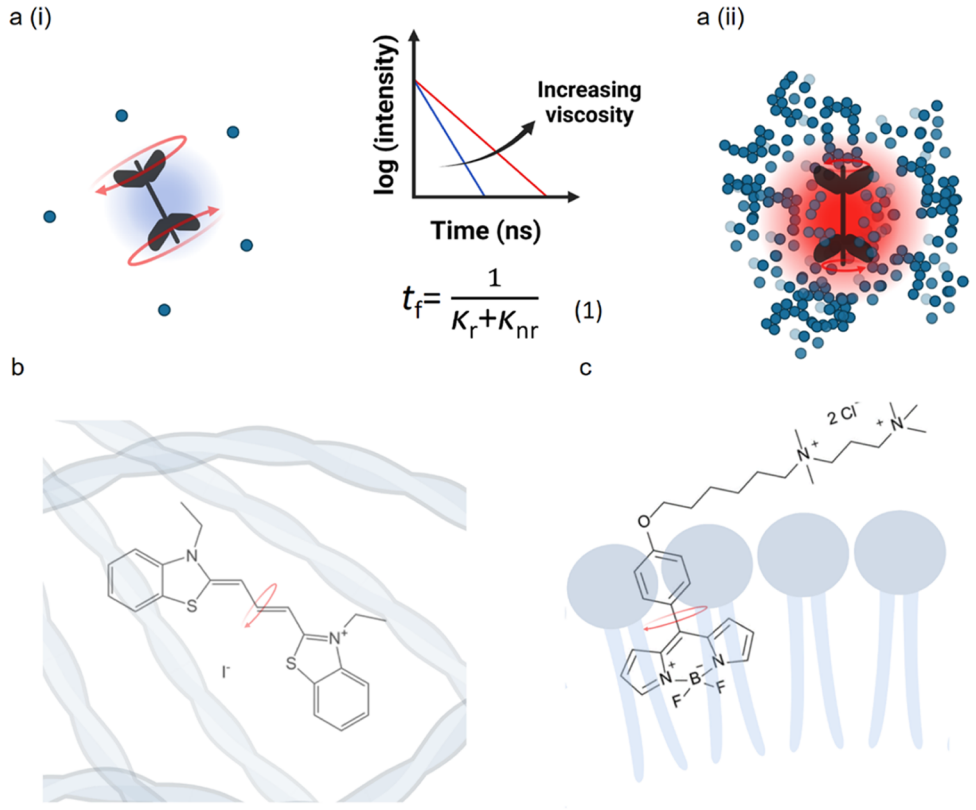


Figure 1. (a (i)) In a less crowded environment (lower viscosity), the intramolecular rotation of a molecular rotor is faster and results in lower fluorescence intensity and lifetime. (a (ii)) In a more crowded environment, due to steric hindrance, the slower intramolecular rotation leads to increased intensity and lifetime values of the rotor. The graph in the middle demonstrates how increasing viscosity affects the time-resolved decay traces of molecular rotors. Blue color corresponds to a lower viscosity environment (lower lifetime), whereas red represents a trace recorded in a more viscous environment (higher lifetime). The equation below (1) describes the relationship of fluorescence lifetime (t_f) with the radiative (κ_r) and nonradiative (κ_{nr}) decay constants, where k_{nr} is affected by molecular crowding. (b) Chemical structure of $DiSC_2(3)$ in an environment of actin assemblies. (c) Chemical structure of BODIPY++ incorporated in a lipid layer. Red arrows indicate the direction of the hypothesized intramolecular rotation.

spatial information without being able to directly elucidate any biophysical and chemical aspects of actin and ABP interactions.

In this study, for the first time, we combine fluorescence lifetime imaging microscopy (FLIM) and environmentally sensitive dyes termed "molecular rotors" to directly measure the viscosity and packing of actin bundles. Furthermore, we use a membrane-localized rotor to directly probe the effect of actin attachment on the viscosity of lipid membranes. The method developed here can thus underpin new studies into the biophysical and structural properties of polymerized actin and its interactions with other cellular components like the lipid membrane.

Molecular rotors are a group of environmentally sensitive synthetic fluorescent molecules that exhibit two competitive relaxation pathways following excitation: radiative decay (leading to fluorescence emission) and intramolecular rotation (leading to nonradiative decay and emission quenching).[17,18] The nonradiative decay is affected by local steric hindrance, *e.g.*, viscosity or crowding, allowing for the emission intensity and lifetime of molecular rotors to serve as microviscosity indicators of their surrounding environment (Figure 1a). Microviscosity is well described by the concept of the solvent free volume: increased concentrations of small solutes result in increased microviscosity (and rotor lifetime values) whereas dilute solutions of large macromolecules do not affect the rotors' signal.[19] FLIM enables the visualization of the spatial distribution of fluorescence lifetime values in every pixel of a sample's image, *via* confocal or multiphoton-excited microscopy.[20−22] Importantly, in contrast to fluorescence intensity, fluorescence lifetime is independent of the fluorophore concentration.[23] Thus, molecular rotors in combination with FLIM constitute a powerful microscopical method suitable to accurately measure the viscosity of microscopic samples, such as synthetic and bacterial lipid membranes, protein aggregates, and cellular organelles.[24−27]

Here, we identified a commercially available cyanine rotor, 3,3-diethylthiacarbocyanine iodide, $DiSC_2(3)$ (Figure 1b), that not only can probe viscosity variations of actin bundles in detail but also can distinguish bundles with different interfilamentous architectures. Following a similar approach, we next used a BODIPY-based rotor (Figure 1c) to monitor lipid viscosity variations upon cross-linking actin assemblies with the lipid membrane of artificial cells. Our method allows, for the first time, to visualize actin packing relevant to structural actin cytoskeletal properties, as well as to monitor downstream mechanical changes of the lipid bilayer following the attachment of polymerizing actin assemblies.

RESULTS

$DiSC_2(3)$ Can Monitor Actin Bundling

$DiSC_2(3)$ has previously been shown to act as a hydrophilic molecular rotor with a strong emission intensity and lifetime

https://doi.org/10.1021/jacsau.4c00237
JACS Au 2024, 4, 2041−2049

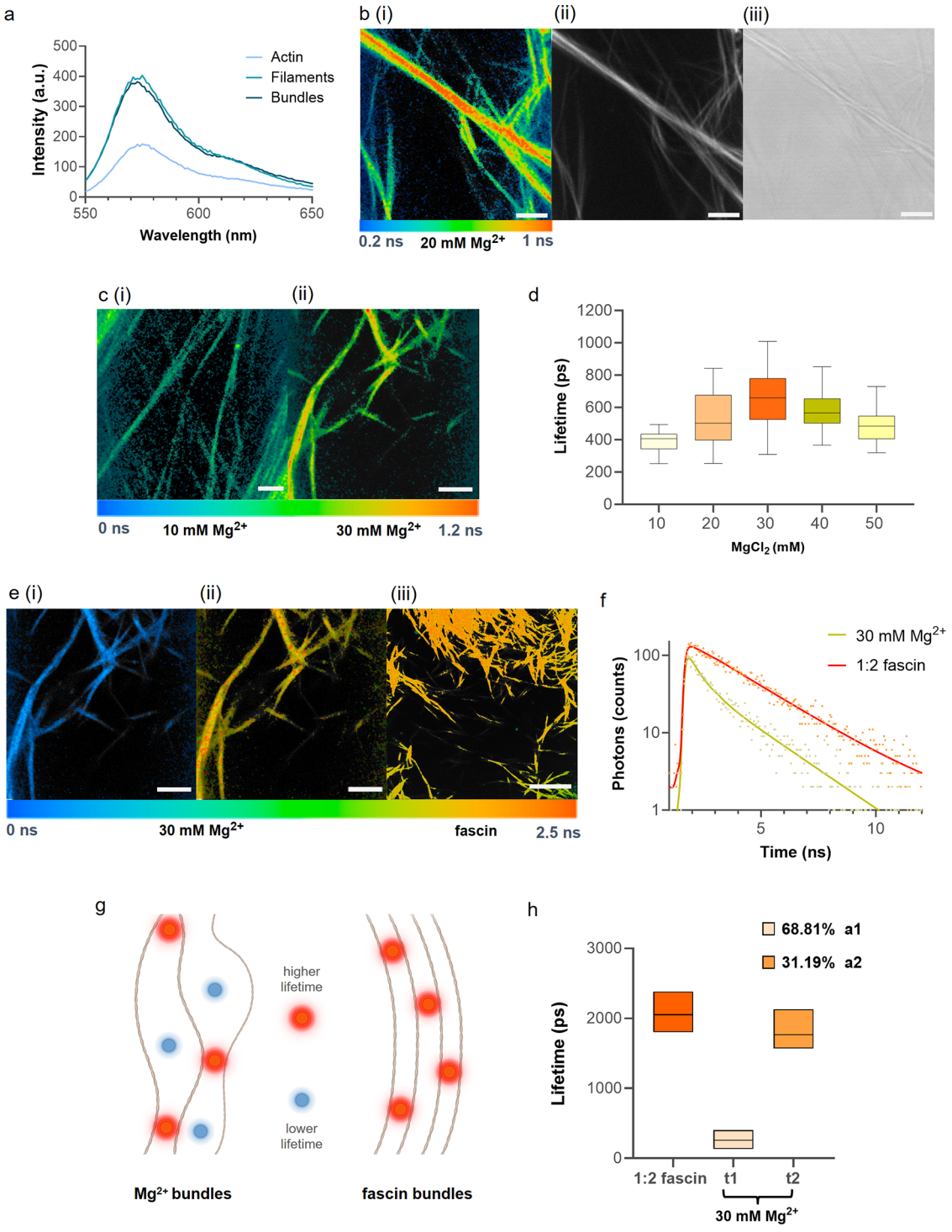


Figure 2. (a) Fluorescence emission spectra of $DiSC_2(3)$ recorded in the presence of actin monomers, actin filaments, and Mg^{2+}-mediated bundles, λ_{exc} 520 nm. (b (i)) FLIM image of 20 mM Mg^{2+}-mediated bundles showing regions of higher and lower viscosities. (b (ii)) Fluorescence intensity and (b (iii)) brightfield images of the same sample. (c) FLIM images of 10 mM Mg^{2+}(ci) and 30 mM Mg^{2+}(cii) bundles; the latter shows higher viscosity. (d) Amplitude-weighted lifetime distribution of bundles formed at varying Mg^{2+} concentrations. Statistical analysis is presented in Figure S4c. Lifetime values from a total of 300 ROIs from FLIM images were analyzed (n = 3 independent repeats). (e) FLIM images of t1 (e (i)) and t2 (e (ii)) of Mg^{2+} bundles in comparison with a single lifetime distribution recorded for fascin bundles (e (iii)). (f) Fluorescence decay traces of 30 mM Mg^{2+}- and fascin-mediated bundles fitted with monoexponential and biexponential models, respectively. (g) Schematic with the proposed model of interaction of $DiSC_2(3)$ and the two types of bundles formed. Mg^{2+} bundle decays were fitted best with two components, implying regions with higher and lower viscosities present, whereas fascin bundle decays were fitted monoexponentially, indicating an ordered interfilamentous structure with a single $DiSC_2(3)$ environment. (h) Comparison of lifetime distribution seen for fascin bundles with distributions seen for Mg^{2+} bundles (n = 3). Mean percentage ratios (amplitudes a1 and a2) of t1 and t2 are also shown. Scale bars in (b, c, e (i), and e (ii)) are 5 μm and in (e (iii)) is 10 μm. For FLIM, λ_{exc} 960, λ_{emis} 520–620 nm.

https://doi.org/10.1021/jacsau.4c00237
JACS Au 2024, 4, 2041−2049

dependence on the surrounding viscosity, and it has been used to monitor viscosity changes in atmospheric aerosols and to detect multiple steps of amyloid aggregation *via* FLIM.[25,28] To assess the ability of $DiSC_2(3)$ to probe actin's polymerization and bundling, we first obtained fluorescence emission spectra of monomeric and filamentous actin, as well as Mg^{2+}-mediated actin bundles, suspended in solution, in quartz cuvettes. Increased fluorescence intensity was recorded for the filamentous and bundled actin samples, suggesting they created a more crowded environment for the added rotor than the monomeric actin state (Figure 2a). To visualize and quantify the viscosity variations within polymerizing actin samples, we next performed FLIM. A typical lifetime image of Mg^{2+}-mediated actin bundles is shown in Figure 2bi and reveals the areas of lower and higher viscosities (lifetimes) within each field of view. A direct comparison with the intensity image (Figure 2bii) shows that bundle regions that appear to be thicker present higher lifetimes, suggesting more packed actin assemblies and vice versa. Colocalization of actin rotor $DiSC_2(3)$ with polymerized actin in Mg^{2+}-induced actin bundles was verified by Förster resonance energy transfer (FRET) microscopy in the presence of both $DiSC_2(3)$ and Acti-stain 670 phalloidin, an actin-targeting peptide that only binds to polymerized actin. $DiSC_2(3)$ served as an FRET donor and was selectively excited at 488 nm. The signal from 670 phalloidin, serving as an FRET acceptor, cannot be detected, unless the FRET donor and acceptor colocalize within <10 nm. An appreciable signal was collected in the acceptor channel at 680−800 nm (Figure S1a,b), showing the colocalization of $DiSC_2(3)$ with polymerized actin bundles. When only 670 phalloidin was present and upon excitation at 488 nm, no signal was observed in the detection range of $DiSC_2(3)$, 520−650 nm (Figure S1c).

We then further explored the sensitivity of $DiSC_2(3)$ toward actin bundling by comparing FLIM measurements obtained for Mg^{2+}- and fascin-mediated bundles. Different concentrations of Mg^{2+} have previously been reported to produce bundles with heterogeneous interfilamentous spacing and varying bending stiffness values, all being less rigid than fascin bundles that are tightly packed and ordered.[29−31] Thus, we produced bundles in a range of Mg^{2+} concentrations (10−50 mM) as well as fascin-induced bundles with a 2:1 molar ratio of actin to fascin. Lifetime values were selected from individual bundles visible in FLIM (Figure S2a). Each of the bundle samples formed under different Mg^{2+} concentrations produced a range of lifetime values (Figure 2d) corresponding to a mixture of bundles with varying viscosities. While $DiSC_2(3)$ displays a monoexponential decay in homogeneous solutions (*e.g.*, methanol/glycerol),[25] fluorescence decays collected from Mg^{2+} bundles were best fitted to a biexponential decay model (Figures 2e and S2e−h), suggesting two distinct environments, with lower (t1) and higher (t2) lifetime values of 135.7 and 2479 ps, respectively, corresponding to less and more crowded bundle regions (Figure 2f−h). The presence of multiple components was also verified with phasor analysis (see Figure S7b). Further analysis of the FLIM data for all Mg^{2+} bundles (Figure S4) indicate that the lifetime values t1 and t2 remain constant between different Mg^{2+} concentrations and correspond to viscosities of *ca.* 1 and 500 mPa·s, according to the rotor calibration obtained in sucrose/water solutions,[28] which was deemed the closest match for the present aqueous-based samples (Figure S5). However, the relative amplitudes of the two components change, with the highest mean value for a1, the faster component, seen for 10 mM Mg^{2+} at 84.82% and the lowest, 68.81%, for 30 mM Mg^{2+}. The short lifetime component closely corresponds to the lifetime seen for $DiSC_2(3)$ in water, thus indicating that some fraction of the dye shows unrestricted rotation within the actin bundles. However, the second fraction characterized by a2 and t2 corresponds to conditions of very high crowding (restricted rotation but not fully bound). Our analysis indicates that increased bundle packing (increased average lifetimes) is a result of the increased ratio of denser to looser regions (a2/a1) within a bundle.

Consequently, of all of the Mg^{2+} concentrations studied, the lowest mean lifetime value was observed for the 10 mM Mg^{2+} sample and the highest for the 30 mM Mg^{2+} sample (Figure 2c,d). This trend is in agreement with the study of Castaneda et al., where TIRF microscopy was used to calculate the bending stiffness of bundles formed under the same range of Mg^{2+} concentrations as employed here,[29] and they further suggested that the rigidity of these bundles is proportional to the microviscosity of their interfilamentous regions.

Next, using the same approach, we explored the influence of fascin on actin bundling. Fascin is a major actin-bundling protein that regulates cell motility and has recently received attention as a promising prognostic marker of metastatic cancer.[32,33] In contrast to Mg^{2+}-mediated bundles, fascin-induced bundles presented monoexponential decays of actin rotor $DiSC_2(3)$ with characteristic lifetimes between 1.8 and 2.4 ns, implying a homogeneous environment for the rotor in the bundle interfilamentous space (Figure 2e,g,h).

Indeed, previous structural studies on fascin bundles have revealed a dense and ordered architecture due to the ability of fascin to cross-link actin with a distinct interfilament distance of 8 nm.[34] These equal interfilament spaces created by fascin bundling of actin (Figure 2g, right) are of a size that is likely to significantly restrict the intramolecular movement of actin rotor $DiSC_2(3)$, but not to completely confine it, preventing its motion. In order to verify that single lifetimes observed in these experiments were not a result of a strong $DiSC_2(3)$ binding to actin or fascin, we performed time-correlated single photon counting (TCSPC) measurements of samples containing only actin or fascin that produced multiexponential decays (Figure S8). We then compared fascin bundles with the 30 mM Mg^{2+} bundles that presented the higher lifetimes among all Mg^{2+} concentrations studied. Analysis of the contribution of the two components of 30 mM Mg^{2+} bundles (Figure S3m,n) revealed that the longer lifetime (t2) values were lower than those observed for fascin bundles (Figure 2f,h), corresponding to viscosities of *ca.* 6000 mPa·s, indicating that even in the most packed Mg^{2+} bundles, the rotor senses larger interfilamentous spaces compared to the ones of 1:2 fascin:actin-mediated bundles. These results agree well with previous studies that report the increased rigidity of ABP-induced bundles against bundles whose filaments are not cross-linked.[35,36]

Encapsulation and Attachment of Actin Networks in GUVs

Having demonstrated that FLIM and molecular rotors can probe actin bundling, we then explored whether we can use FLIM to reveal the mechanical effects of actin assemblies on lipid membranes. It is well known that cytoskeleton components can affect the diffusion of species within the lipid bilayers in cells, for example in a "picket and fence" model or when actin attachment can induce lipid phase separa-

https://doi.org/10.1021/jacsau.4c00237
JACS Au 2024, 4, 2041−2049

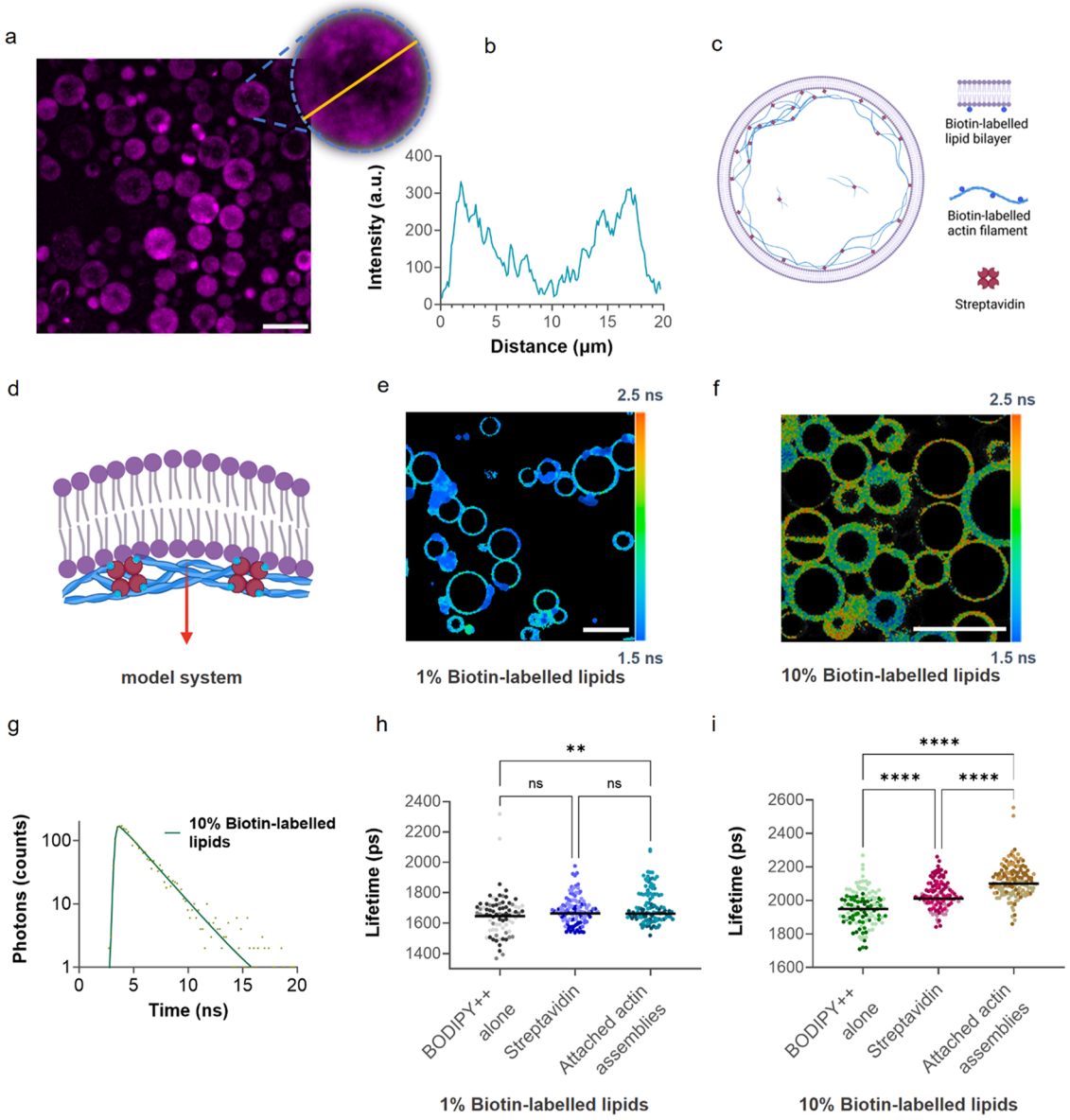


Figure 3. (a) Confocal microscopy image of GUVs (90:10 DOPC:Biotinyl Cap PE) with actin assemblies attached to the inner lipid monolayer. Inset presents a magnified GUV (dashed circle) where actin appears to be localized at the inner periphery of the liposome. 10% mol^{-1} of actin was rhodamine-labeled, 514 nm excitation, 550−650 nm detection. (b) Fluorescence intensity profile of the yellow line across the GUV from inset of (a) where the two peaks of high intensity represent the attachment of actin to the lipid membrane. (c) Schematic presenting the architecture of GUVs with attached actin assemblies and (d) the proposed pulling force (red arrow) of actin assemblies on the lipid layer that should result in a more viscous lipid membrane. (e) FLIM image of 1% biotin-labeled lipid GUVs with attached actin assemblies. (f) FLIM image of 10% biotin-labeled lipid GUVs with attached actin assemblies, 488 nm excitation, 500−600 nm detection. (g) A typical fluorescence decay trace recorded for BODIPY++ incorporated into 10% biotin-labeled lipid GUVs in the presence of actin. Traces were fitted by a monoexponential decay model, consistent with the absence of rotor aggregates in the sample. (h) Lifetime distribution of BODIPY++ in 1% biotin-labeled GUVs, with streptavidin and with attached actin assemblies (376 GUVs analyzed). (i) Lifetime distribution of BODIPY++ with 10% biotin-labeled GUVS (301 GUVs analyzed). All three conditions are significantly different (nonparametric one-way ANOVA, ****: $P < 0.0001$) and GUVs with attached actin assemblies present the highest lifetime values. A total of 677 GUVs were analyzed in three independent repeats, shown as points with different shades of the same color in panels (f, g);. Scale bars at (a, e, f) are 20 μm.

tion.[37,38] In our artificial cell model system, we used emulsion phase transfer (EPT) to form GUVs and encapsulate the necessary components for actin networks to form and attach to the inner lipid monolayer. EPT is a well-established method of forming GUVs that offers control of the composition of the encapsulated solution mixture.[39,40] Aqueous solutions were osmotically balanced with 0.5 M glucose (outer) and 0.5 M maltotriose (inner) in 1× polymerization buffer. We choose to use maltotriose for the inner solution, as its higher density and mass compared to sucrose, which is usually used in EPT, increased the yield of formed liposomes and reduced their movement during FLIM measurements, increasing the signal-to-noise ratio of accumulated data. Networks were formed and attached to the inner lipid monolayer by streptavidin that cross-linked both biotin-labeled actin and biotin-labeled lipids, as was confirmed by fluorescence imaging (Figure 3a). For all experiments, we used a 1:200 ratio of actin to biotin-labeled actin and 2.5 μM streptavidin. Formation of actin networks

https://doi.org/10.1021/jacsau.4c00237
JACS Au 2024, 4, 2041−2049

upon encapsulation was confirmed in a large vesicle population with confocal microscopy, although the distribution from vesicle to vesicle did vary, with some liposomes presenting localization of actin to the periphery of the inner lipid layer and others presenting a homogeneous encapsulation in the bulk (Figure 3b,c).

Actin Attachment Increases Lipid Packing Density of the Bilayer

We used a bilayer-localized BODIPY++ molecular rotor[41] (Figure 1c) to investigate the effects of attaching actin networks to the inner lipid monolayer. By combining DOPC and 18:1 Biotinyl Cap PE lipids, we created two conditions at which actin attached to the bilayer: (i) a strong membrane attachment condition in the presence of 10% biotin-labeled lipids and (ii) a weak condition with 1% biotin-labeled lipids. It has been previously reported that streptavidin and avidin attachment to the lipid bilayer increases the membrane rigidity of GUVs.[42] Thus, for each set of experiments, we also measured two control conditions, one with no proteins added and the other one with streptavidin alone. BODIPY++ is known to localize in the hydrophobic tail region of lipid bilayers, and has previously been extensively used to characterize the packing (microviscosity) of the biological bilayers, whereby monoexponential decays of the rotor can be directly correlated to the viscosity of the fluid lipid phase that it localizes in.[24,41,43]

FLIM analysis was performed on individual GUVs, producing averaged lifetime values for each selected GUV of the FLIM image (Figure S9a). All fluorescence decays fitted well with a monoexponential model (Figures 3g and S9d), indicating good incorporation of the rotor into a single-phase liquid disordered membrane[44] and absence of dye aggregates that prevent the direct correlation of the rotor's lifetime with the membrane viscosity.[45]

In weak actin-binding conditions, GUVs with attached actin networks presented the highest lifetime values (Table S1) but no statistical difference between the actin-attached samples and the controls was observed (Figure 3h). However, when the ratio of biotin-labeled lipids was increased to 10% (strong binding conditions), lifetimes of the rotor from GUVs with attached actin were significantly higher than GUVs encapsulating streptavidin or membrane rotor BODIPY++ alone (Figure 3i). While we note that the presence of the higher ratio of biotin-labeled lipids (both with and without streptavidin) also resulted in increased lifetimes compared to the 1% biotin-labeled composition (increase of *ca.* 350 ps and *ca.* 300 ps, respectively), the presence of actin resulted in the biggest change (*ca.* 400 ps further increase). The resulting viscosities that were calculated from the previously determined rotor calibration[28] are listed in Table S1 and indicate the biggest difference of 98 mPa·s between various conditions tested. These results demonstrate directly how actin assemblies can affect the mechanical properties of lipid membranes.

DISCUSSION

In recent years, the research of cytoskeletal properties and their association with normal and abnormal cell function has significantly contributed to the fields of cell biology and medicine. In addition to live cell research, *in vitro* studies and the application of synthetic cell models have successfully supplemented this effort.[46−49] Elucidating the biophysical properties as well as the complex interactions of the cytoskeleton with other cell components such as the plasma membrane will not only reveal key structural and functional aspects of such interactions but also help us to better understand actin-related diseases and cancer. While the use of electron and fluorescence microscopies is inextricably linked with research in the field, it usually provides one-dimensional information (*e.g.*, fluorescence intensity-based localization of cytoskeletal components) and can have limitations when applied to *in vivo* samples when using electron microscopies.

Here, by using molecular rotors, we present a FLIM-based approach to study actin packing and the effects of actin attachment to lipid membranes in artificial cells. Dynamic alterations in both environments, actin and lipid bilayers, are relevant in many diseases, and their control could also be important in the design of artificial cells. Uniquely, the packing and microstructure of both environments could be revealed by utilizing our approach of combining environmentally sensitive molecular rotors and FLIM.

We demonstrated how actin rotor $DiSC_2(3)$ can efficiently monitor and distinguish the microenvironment of two different actin bundle architectures, Mg^{2+}- and fascin-mediated bundles, by displaying a wide range of lifetimes (0.25−2.37 ns, corresponding to viscosities of 1−6000 mPa·s), assigned to different bundling conditions and actin morphologies. The recorded wide lifetime ranges for $DiSC_2(3)$, well below the "saturation" lifetime corresponding to the immobile rotor, also imply a weak interaction between the rotor and actin, enabling its high sensitivity to the crowding in its surrounding environment rather than as a binding conformation probe. The low affinity of $DiSC_2(3)$ to proteins has also been reported while using FLIM and molecular rotors to monitor amyloid aggregation.[25]

We must note that due to the diffraction-limited resolution of our technique, single filaments of actin could not be resolved with FLIM, but the increased fluorescence intensity of actin rotor $DiSC_2(3)$ in its presence (Figure 2a) indicates that the rotor is also responsive to that type of actin assemblies. However, the combination of FLIM with super-resolution microscopy, such as stimulated emission depletion (STED)-FLIM, and more sensitive detectors, could be promising for probing finer actin assemblies like thin actin networks and filaments.

By forming and cross-linking a minimal actin cortex to the inner lipid monolayer of GUVs with streptavidin, we used a lipid bilayer-specific molecular rotor, BODIPY++, to investigate potential viscosity variations of the lipid membrane in two attachment conditions. The weak attachment condition (1% biotin-labeled lipids) produced lifetime values with no statistical significance between the controls and GUVs encapsulating actin assemblies. For the strong attachment condition (10% biotin-labeled lipids), membrane rotor BODIPY++ reported higher lifetime values upon actin attachment than GUVs encapsulating the rotor and streptavidin alone, presumably due to actin polymerization and the increased number of adhesion points to the membrane. Generation of membrane tension has previously been proposed in liposomal systems encapsulating actomyosin networks.[47] However, our results indicate an increased membrane viscosity as a result of actin attachment alone. Indeed, in live cells, the myosin-independent role of actin and adhesion dynamics on membrane tension, especially during cell migration and endocytosis, is well established and has been

https://doi.org/10.1021/jacsau.4c00237
JACS Au 2024, 4, 2041−2049

described in both experimental and computational studies.[50−53]

Lastly, the membrane of GUVs formed with 10% biotin-labeled lipids exhibited significantly higher lifetime values than the 1% composition, even in the absence of actin and streptavidin (Figure 3f,g). We attributed this effect to the increased ratio of 18:1 Biotinyl Cap PE lipids that have bulkier headgroups than DOPC lipids. As previously reported, the presence of lipids with large headgroups (*e.g.*, glycolipids, PEG-lipids) can increase the rigidity of model and live cell membranes.[54−56]

We emphasize that this study represents the first instance of using fluorescence lifetime microscopy to measure differences in the biophysical properties of actin assemblies and their effects on lipid membranes. Considering the widespread use of this technique, its sensitivity, and the spatial information it provides, our results represent a significant advancement. This is especially true when coupled with the biomedical significance of actin biophysics and our relatively limited understanding of it, attributable to the deficiencies of existing techniques.

To conclude, we believe that our results pave the way for using FLIM and molecular rotors to monitor actin dynamics and its interactions with lipid membranes. This method can be directly applied to both *in vitro* and *in vivo* cytoskeletal studies of the membrane BODIPY++ rotor. Application of actin rotor $DiSC_2(3)$ could be extended to experiments in live cells upon attachment to actin-targeting compounds.[57] Our approach has the potential to provide important insights into both biophysical and morphological aspects of actin and its interactions with lipid membranes, not only in cell structural and motility studies but also in the field of actin-related diseases and cancer.

METHODS

All standard chemicals were purchased from Sigma-Aldrich and were used without further purification. Monomeric, rhodamine and biotin-labeled actin, fascin, and Acti-stain 670 phalloidin were purchased from Cytoskeleton. Streptavidin (recombinant) was purchased from Thermo Scientific. All lipids were purchased from Avanti Polar Lipids: 1,2-dioleoyl-*sn*-glycero-3-phosphocholine (DOPC), 1,2-dioleoyl-*sn*-glycero-3-phosphoethanolamine-*N*-(cap biotinyl) (18:1 Biotinyl Cap PE). Lipid stock solutions were prepared by dissolving lipid powders in chloroform to a concentration of 25 mg mL^{-1} and were stored at −20 °C. BODIPY++ rotor was previously synthesized according to ref 31, and $DiSC_2(3)$ rotor (99% purity) was purchased from Strateck Scientific.

Actin Samples Preparation

Monomeric actin was polymerized to a final concentration of 23.4 μM (1 mg mL^{-1}) with 10% of 10× polymerization buffer [1 M KCl, 20 mM $MgCl_2$, 10 mM EGTA, 0.2 M HEPES−KOH (pH 7.5)] in the presence of 1 mM ATP following standard protocols.[58] For Mg^{2+}-mediated bundles, the actin mixture was supplemented with varying $MgCl_2$ concentrations diluted from a 100 mM stock solution in water. $DiSC_2(3)$ was used at 23.4 μM for all samples as the optimal concentration for the microscopy setup used (Figure S10a). For fascin-induced bundling, 11.7 μM fascin were added to the mixture (2:1 actin: fascin molar ratio) (Figure S10b). For FRET microscopy measurements, Acti-stain 670 was used at 1.2 μM.

Formation of Giant Unilamellar Vesicles and Attachment of Actin Networks

GUVs were produced with an EPT protocol described by Chiba et al. with slight modifications.[59] At first, lipid films of 5 mg of lipids were prepared by mixing DOPC and 18:1 Biotinyl Cap PE chloroform solutions in glass phials and dried under a $N_2(g)$ flow. Subsequently, lipid films were stored under vacuum for at least 3 h at room temperature before use to ensure total chloroform evaporation. Lipid in oil mixtures were then prepared by dissolving lipid films in mineral oil (5 mg mL^{-1}) and sonicated for 60 min at 50 °C. Emulsion droplets were formed by mixing 200 μL of lipid in oil with 20 μL of the solution to be encapsulated inside the GUVs. For control experiments, only maltotriose (0.5 M) and BODIPY++ (0.5 μM) with/without streptavidin (2.5 μM) were encapsulated. For attached actin networks, the inside solution also contained 23.4 μM actin, 0.5% of which was biotin-labeled, 1× polymerization buffer, and 1 mM ATP. The emulsion was then layered above 250 μL of 0.5 M glucose in 1× buffer in 1.5 mL Eppendorf tubes that were centrifuged for 30 min at 10,000 rpm. After centrifugation, the supernatant was removed, and sedimented GUVs were resuspended in 100 μL of 0.5 M glucose. Samples were then transferred in plasma desorption mass spectrometry (PDMS) chambers and incubated for at least 15 min at room temperature to allow for BODIPY++ to incorporate in the lipid bilayer and GUVs to settle before microscopy measurements.

Fluorescence Lifetime Imaging Microscopy (FLIM)

FLIM measurements were performed in a confocal SP5 II microscope (Leica Microsystems) equipped with a TCSPC card (SPC-830, Becker and Hickl) using either a 63× water immersion objective (NA: 1.2) or a 100× oil immersion (NA:1.4) objective with correction collars. The image resolution was 256 × 256 pixels. Actin samples containing $DiSC_2(3)$ were excited at 960 nm using a Ti: Sapphire pulsed laser (Chameleon Vision II, Coherent). $DiSC_2(3)$ emission was recorded between 520 and 650 nm. Liposome samples containing BODIPY++ were excited at 477 nm with a pulsed diode laser (Becker and Hickl GmbH), and emission was collected from 500 to 600 nm. Actin bundle samples (10 μL) were placed on a 24 mm × 50 mm cover glass and sealed with an 18 mm × 18 mm coverslip. For liposome samples, a square 15 mm × 15 mm PDMS chamber was used between the coverslips. SPCImage software (Becker and Hickl) was used to fit fluorescence decays and generate FLIM images. Time-resolved decay traces were fitted using mono- or biexponential decay model. In case of the biexponential decays, average lifetime values were amplitude-weighted and were calculated according to eq 1

$$t_m = \frac{\sum_{i=1}^{n} a_i t_i}{\sum_{i=1}^{n} a_i} \quad (1)$$

where a is the amplitude and t is the lifetime of the ith component. Lifetime values from single bundles and liposomes were extracted using the software's masking tool (area mode), and graphs were plotted and analyzed with Prism (GraphPad Software).

Fluorescence Emission Spectra and Lifetime Measurements

Emission spectra were recorded on a Cary Eclipse fluorescence spectrophotometer (Agilent Technologies). $DiSC_2(3)$ samples were placed in 10 μL, 10 mm path length quartz microcuvettes (Starna Scientific) and excited at 520 nm. Emission spectra were recorded between 550 and 700 nm and corrected for the detector sensitivity. Fluorescence decay traces of $DiSC_2(3)$ samples were acquired by using a DeltaFlex TCSPC lifetime fluorometer (Horiba Scientific). Excitation was performed with a NanoLED-L 470 nm pulsed laser diode (Horiba Scientific) and detection was set at 570 ± 32 nm. Acquisition was continued until 10,000 peak counts, and the data was analyzed with DAS6 decay analysis software (Horiba Scientific).

ASSOCIATED CONTENT

Supporting Information

The Supporting Information is available free of charge at https://pubs.acs.org/doi/10.1021/jacsau.4c00237.

FRET colocalization results; detailed FLIM analysis; full data for lifetime distributions; calibration of molecular

https://doi.org/10.1021/jacsau.4c00237
JACS Au 2024, 4, 2041−2049

rotor lifetimes; phasor analysis data; fluorescence decay traces; data analysis details (PDF)

AUTHOR INFORMATION

Corresponding Authors

Nickolas J. Brooks − *Department of Chemistry, Imperial College London, Molecular Sciences Research Hub, London W12 0BZ, U.K.*; Email: n.brooks@imperial.ac.uk

Marina K. Kuimova − *Department of Chemistry, Imperial College London, Molecular Sciences Research Hub, London W12 0BZ, U.K.*; orcid.org/0000-0003-2383-6014; Email: m.kuimova@imperial.ac.uk

Yuval Elani − *Department of Chemical Engineering, Imperial College London, London SW7 2AZ, U.K.*; orcid.org/0000-0002-9603-2490; Email: y.elani@imperial.ac.uk

Author

Ion A. Ioannou − *Department of Chemistry, Imperial College London, Molecular Sciences Research Hub, London W12 0BZ, U.K.; Department of Chemical Engineering, Imperial College London, London SW7 2AZ, U.K.*; orcid.org/0000-0001-8749-1049

Complete contact information is available at: https://pubs.acs.org/10.1021/jacsau.4c00237

Author Contributions

CRediT: **Ion A. Ioannou** conceptualization, data curation, formal analysis, methodology, resources, software, validation, visualization, writing-original draft, writing-review & editing; **Nicholas J Brooks** conceptualization, funding acquisition, supervision, writing-review & editing; **Marina K. Kuimova** conceptualization, funding acquisition, project administration, supervision, writing-review & editing; **Yuval Elani** conceptualization, funding acquisition, project administration, supervision, writing-review & editing.

Notes

The authors declare no competing financial interest.

ACKNOWLEDGMENTS

M.K.K. acknowledges the Engineering and Physical Sciences Research Council (EPSRC) for a Career Acceleration Fellowship (EP/I003983/1). Y.E. acknowledges the support of a UKRI Future Leaders Fellowship (MR/S031537/1). I.A.I. acknowledges the support of a studentship from the Leverhulme Doctoral Scholarship Program in Cellular Bionics. I.A.I. would also like to acknowledge Drs PS Sherin and M Páez-Pérez for useful discussions.

REFERENCES

(1) Dominguez, R.; Holmes, K. C. Actin structure and function. *Annu. Rev. Biophys.* **2011**, *40*, 169−186.

(2) Pollard, T. D. Actin and Actin-Binding Proteins. *Cold Spring Harbor Perspect. Biol.* **2016**, *8*, No. a018226.

(3) dos Remedios, C. G.; Chhabra, D.; Kekic, M.; Dedova, I. V.; Tsubakihara, M.; Berry, D. A.; Nosworthy, N. J. Actin binding proteins: regulation of cytoskeletal microfilaments. *Physiol. Rev.* **2003**, *83* (2), 433−473.

(4) Rottner, K.; Faix, J.; Bogdan, S.; Linder, S.; Kerkhoff, E. Actin assembly mechanisms at a glance. *J. Cell Sci.* **2017**, *130* (20), 3427−3435.

(5) Clarkson, E.; Costa, C. F.; Machesky, L. M. Congenital myopathies: diseases of the actin cytoskeleton. *J. Pathol.* **2004**, *204* (4), 407−417.

(6) Finsterer, J.; Stöllberger, C. Primary myopathies and the heart. *Scand. Cardiovasc. J.* **2008**, *42* (1), 9−24.

(7) Grothey, A.; Hashizume, R.; Sahin, A. A.; McCrea, P. D. Fascin, an actin-bundling protein associated with cell motility, is upregulated in hormone receptor negative breast cancer. *Br. J. Cancer* **2000**, *83* (7), 870−873.

(8) Al-Alwan, M.; Olabi, S.; Ghebeh, H.; Barhoush, E.; Tulbah, A.; Al-Tweigeri, T.; Ajarim, D.; Adra, C. Fascin is a key regulator of breast cancer invasion that acts via the modification of metastasis-associated molecules. *PLoS One* **2011**, *6* (11), No. e27339.

(9) McKayed, K. K.; Simpson, J. C. Actin in action: imaging approaches to study cytoskeleton structure and function. *Cells* **2013**, *2* (4), 715−731.

(10) Small, J.; Rottner, K.; Hahne, P.; Anderson, K. I. Visualising the actin cytoskeleton. *Microsc. Res. Tech.* **1999**, *47* (1), 3−17.

(11) Jung, M.; Kim, D.; Mun, J. Y. Direct Visualization of Actin Filaments and Actin-Binding Proteins in Neuronal Cells. *Front. Cell Dev. Biol.* **2020**, *8*, No. 588556.

(12) Gwosch, K. C.; Pape, J. K.; Balzarotti, F.; Hoess, P.; Ellenberg, J.; Ries, J.; Hell, S. W. MINFLUX nanoscopy delivers 3D multicolor nanometer resolution in cells. *Nat. Methods* **2020**, *17* (2), 217−224.

(13) Betzig, E.; Patterson, G. H.; Sougrat, R.; Lindwasser, O. W.; Olenych, S.; Bonifacino, J. S.; Davidson, M. W.; Lippincott-Schwartz, J.; Hess, H. F. Imaging intracellular fluorescent proteins at nanometer resolution. *Science* **2006**, *313* (5793), 1642−1645.

(14) Huang, B.; Bates, M.; Zhuang, X. Super-resolution fluorescence microscopy. *Annu. Rev. Biochem.* **2009**, *78*, 993−1016.

(15) Mihaila, T. S.; Bäte, C.; Ostersehlt, L. M.; Pape, J. K.; Keller-Findeisen, J.; Sahl, S. J.; Hell, S. W. Enhanced incorporation of subnanometer tags into cellular proteins for fluorescence nanoscopy via optimized genetic code expansion. *Proc. Natl. Acad. Sci. U.S.A.* **2022**, *119* (29), No. e2201861119.

(16) Melak, M.; Plessner, M.; Grosse, R. Actin visualization at a glance. *J. Cell Sci.* **2017**, *130* (3), 525−530.

(17) Haidekker, M. A.; Theodorakis, E. A. Molecular rotors–fluorescent biosensors for viscosity and flow. *Org. Biomol. Chem.* **2007**, *5* (11), 1669−1678.

(18) Kuimova, M. K. Mapping viscosity in cells using molecular rotors. *Phys. Chem. Chem. Phys.* **2012**, *14* (37), 12671−12686.

(19) Páez-Pérez, M.; Kuimova, M. K. Molecular Rotors: Fluorescent Sensors for Microviscosity and Conformation of Biomolecules. *Angew. Chem., Int. Ed.* **2024**, *63* (6), No. e202311233.

(20) Chang, C. W.; Sud, D.; Mycek, M. A. Fluorescence lifetime imaging microscopy. *Methods Cell Biol.* **2007**, *81*, 495−524.

(21) van Munster, E. B.; Gadella, T. W.Fluorescence lifetime imaging microscopy (FLIM). In *Microscopy Techniques*; Springer, 2005; Vol. *95*, pp 143−175.

(22) Trinh, A. L.; Ber, S.; Howitt, A.; Valls, P. O.; Fries, M. W.; Venkitaraman, A. R.; Esposito, A. Fast single-cell biochemistry: theory, open source microscopy and applications. *Methods Appl. Fluoresc.* **2019**, *7* (4), No. 044001.

(23) Datta, R.; Heaster, T. M.; Sharick, J. T.; Gillette, A. A.; Skala, M. C. Fluorescence lifetime imaging microscopy: fundamentals and advances in instrumentation, analysis, and applications. *J. Biomed. Opt.* **2020**, *25* (7), No. 071203, DOI: 10.1117/1.JBO.25.7.071203.

(24) Mika, J. T.; Thompson, A. J.; Dent, M. R.; Brooks, N. J.; Michiels, J.; Hofkens, J.; Kuimova, M. K. Measuring the Viscosity of the *Escherichia coli* Plasma Membrane Using Molecular Rotors. *Biophys. J.* **2016**, *111* (7), 1528−1540.

(25) Thompson, A. J.; Herling, T. W.; Kubánková, M.; Vyšniauskas, A.; Knowles, T. P.; Kuimova, M. K. Molecular Rotors Provide Insights into Microscopic Structural Changes During Protein Aggregation. *J. Phys. Chem. B* **2015**, *119* (32), 10170−10179.

(26) Chambers, J. E.; Kubánková, M.; Huber, R. G.; López-Duarte, I.; Avezov, E.; Bond, P. J.; Marciniak, S. J.; Kuimova, M. K. An Optical

Technique for Mapping Microviscosity Dynamics in Cellular Organelles. *ACS Nano* **2018**, *12* (5), 4398−4407.
(27) Páez-Pérez, M.; López-Duarte, I.; Vyšniauskas, A.; Brooks, N. J.; Kuimova, M. K. Imaging non-classical mechanical responses of lipid membranes using molecular rotors. *Chem. Sci.* **2021**, *12* (7), 2604−2613.
(28) Hosny, N. A.; Fitzgerald, C.; Vyšniauskas, A.; Athanasiadis, A.; Berkemeier, T.; Uygur, N.; Pöschl, U.; Shiraiwa, M.; Kalberer, M.; Pope, F. D.; Kuimova, M. K. Direct imaging of changes in aerosol particle viscosity upon hydration and chemical aging. *Chem. Sci.* **2016**, *7* (2), 1357−1367.
(29) Castaneda, N.; Zheng, T.; Rivera-Jacquez, H. J.; Lee, H. J.; Hyun, J.; Balaeff, A.; Huo, Q.; Kang, H. Cations Modulate Actin Bundle Mechanics, Assembly Dynamics, and Structure. *J. Phys. Chem. B* **2018**, *122* (14), 3826−3835.
(30) Jansen, S.; Collins, A.; Yang, C.; Rebowski, G.; Svitkina, T.; Dominguez, R. Mechanism of actin filament bundling by fascin. *J. Biol. Chem.* **2011**, *286* (34), 30087−30096.
(31) Haviv, L.; Gov, N.; Ideses, Y.; Bernheim-Groswasser, A. Thickness distribution of actin bundles in vitro. *Eur. Biophys. J.* **2008**, *37* (4), 447−454.
(32) Jayo, A.; Parsons, M. Fascin: a key regulator of cytoskeletal dynamics. *Int. J. Biochem. Cell Biol.* **2010**, *42* (10), 1614−1617.
(33) Lin, S.; Taylor, M. D.; Singh, P. K.; Yang, S. How does fascin promote cancer metastasis? *FEBS J.* **2021**, *288* (5), 1434−1446.
(34) Winkelman, J. D.; Suarez, C.; Hocky, G. M.; Harker, A. J.; Morganthaler, A. N.; Christensen, J. R.; Voth, G. A.; Bartles, J. R.; Kovar, D. R. Fascin- and alpha-Actinin-Bundled Networks Contain Intrinsic Structural Features that Drive Protein Sorting. *Curr. Biol.* **2016**, *26* (20), 2697−2706.
(35) Shin, J. H.; Mahadevan, L.; So, P. T.; Matsudaira, P. Bending stiffness of a crystalline actin bundle. *J. Mol. Biol.* **2004**, *337* (2), 255−261.
(36) Takatsuki, H.; Bengtsson, E.; Månsson, A. Persistence length of fascin-cross-linked actin filament bundles in solution and the in vitro motility assay. *Biochim. Biophys. Acta, Gen. Subj.* **2014**, *1840* (6), 1933−1942.
(37) Ritchie, K.; Iino, R.; Fujiwara, T.; Murase, K.; Kusumi, A. The fence and picket structure of the plasma membrane of live cells as revealed by single molecule techniques (Review). *Mol. Membr. Biol.* **2003**, *20* (1), 13−18.
(38) Liu, A. P.; Fletcher, D. A. Actin polymerization serves as a membrane domain switch in model lipid bilayers. *Biophys. J.* **2006**, *91* (11), 4064−4070.
(39) Pautot, S.; Frisken, B. J.; Weitz, D. A. Production of Unilamellar Vesicles Using an Inverted Emulsion. *Langmuir* **2003**, *19* (7), 2870−2879.
(40) Fujii, S.; Matsuura, T.; Sunami, T.; Nishikawa, T.; Kazuta, Y.; Yomo, T. Liposome display for in vitro selection and evolution of membrane proteins. *Nat. Protoc.* **2014**, *9* (7), 1578−1591.
(41) López-Duarte, I.; Vu, T. T.; Izquierdo, M. A.; Bull, J. A.; Kuimova, M. K. A molecular rotor for measuring viscosity in plasma membranes of live cells. *Chem. Commun.* **2014**, *50* (40), 5282−5284.
(42) Dieluweit, S.; Csiszár, A.; Rubner, W.; Fleischhauer, J.; Houben, S.; Merkel, R. Mechanical properties of bare and protein-coated giant unilamellar phospholipid vesicles. A comparative study of micropipet aspiration and atomic force microscopy. *Langmuir* **2010**, *26* (13), 11041−11049.
(43) Sherin, P. S.; Vyšniauskas, A.; López-Duarte, I.; Ogilby, P. R.; Kuimova, M. K. Visualising UV-A light-induced damage to plasma membranes of eye lens. *J. Photochem. Photobiol., B* **2021**, *225*, No. 112346.
(44) Dent, M. R.; López-Duarte, I.; Dickson, C. J.; Geoghegan, N. D.; Cooper, J. M.; Gould, I. R.; Krams, R.; Bull, J. A.; Brooks, N. J.; Kuimova, M. K. Imaging phase separation in model lipid membranes through the use of BODIPY based molecular rotors. *Phys. Chem. Chem. Phys.* **2015**, *17* (28), 18393−18402.
(45) Wu, Y.; Štefl, M.; Olzyńska, A.; Hof, M.; Yahioglu, G.; Yip, P.; Casey, D. R.; Ces, O.; Humpolíčková, J.; Kuimova, M. K. Molecular rheometry: direct determination of viscosity in Lo and Ld lipid phases via fluorescence lifetime imaging. *Phys. Chem. Chem. Phys.* **2013**, *15* (36), 14986−14993.
(46) Carvalho, K.; Tsai, F. C.; Lees, E.; Voituriez, R.; Koenderink, G. H.; Sykes, C. Cell-sized liposomes reveal how actomyosin cortical tension drives shape change. *Proc. Natl. Acad. Sci. U.S.A.* **2013**, *110* (41), 16456−16461.
(47) Loiseau, E.; Schneider, J. A.; Keber, F. C.; Pelzl, C.; Massiera, G.; Salbreux, G.; Bausch, A. R. Shape remodeling and blebbing of active cytoskeletal vesicles. *Sci. Adv.* **2016**, *2* (4), No. e1500465.
(48) Kusters, R.; Simon, C.; Dos Santos, R. L.; Caorsi, V.; Wu, S.; Joanny, J. F.; Sens, P.; Sykes, C. Actin shells control buckling and wrinkling of biomembranes. *Soft Matter* **2019**, *15* (47), 9647−9653, DOI: 10.1039/C9SM01902B.
(49) Schmoller, K. M.; Lieleg, O.; Bausch, A. R. Structural and viscoelastic properties of actin/filamin networks: cross-linked versus bundled networks. *Biophys. J.* **2009**, *97* (1), 83−89.
(50) Akamatsu, M.; Vasan, R.; Serwas, D.; Ferrin, M. A.; Rangamani, P.; Drubin, D. G. Principles of self-organization and load adaptation by the actin cytoskeleton during clathrin-mediated endocytosis. *eLife* **2020**, *9*, No. e49840.
(51) Craig, E. M.; Van Goor, D.; Forscher, P.; Mogilner, A. Membrane tension, myosin force, and actin turnover maintain actin treadmill in the nerve growth cone. *Biophys. J.* **2012**, *102* (7), 1503−1513.
(52) Skruzny, M.; Brach, T.; Ciuffa, R.; Rybina, S.; Wachsmuth, M.; Kaksonen, M. Molecular basis for coupling the plasma membrane to the actin cytoskeleton during clathrin-mediated endocytosis. *Proc. Natl. Acad. Sci. U.S.A.* **2012**, *109* (38), E2533−E2542.
(53) Le Clainche, C.; Carlier, M. F. Regulation of actin assembly associated with protrusion and adhesion in cell migration. *Physiol. Rev.* **2008**, *88* (2), 489−513.
(54) Abou-Saleh, R. H.; Swain, M.; Evans, S. D.; Thomson, N. H. Poly(ethylene glycol) lipid-shelled microbubbles: abundance, stability, and mechanical properties. *Langmuir* **2014**, *30* (19), 5557−5563.
(55) Kanduč, M.; Schlaich, A.; de Vries, A. H.; Jouhet, J.; Maréchal, E.; Demé, B.; Netz, R. R.; Schneck, E. Tight cohesion between glycolipid membranes results from balanced water-headgroup interactions. *Nat. Commun.* **2017**, *8*, No. 14899.
(56) Melikishvili, S.; Poturnayova, A.; Ionov, M.; Bryszewska, M.; Vary, T.; Cirak, J.; Muñoz-Fernández, M. A.; Gomez-Ramirez, R.; de la Mata, F. J.; Hianik, T. The effect of polyethylene glycol-modified lipids on the interaction of HIV-1 derived peptide-dendrimer complexes with lipid membranes. *Biochim. Biophys. Acta, Biomember.* **2016**, *1858* (12), 3005−3016.
(57) Kubánková, M.; López-Duarte, I.; Bull, J. A.; Vadukul, D. M.; Serpell, L. C.; de Saint Victor, M.; Stride, E.; Kuimova, M. K. Probing supramolecular protein assembly using covalently attached fluorescent molecular rotors. *Biomaterials* **2017**, *139*, 195−201.
(58) Ono, S. Basic Methods to Visualize Actin Filaments In Vitro Using Fluorescence Microscopy for Observation of Filament Severing and Bundling. *Methods Mol. Biol.* **2016**, *1365*, 187−193.
(59) Chiba, M.; Miyazaki, M.; Ishiwata, S. Quantitative analysis of the lamellarity of giant liposomes prepared by the inverted emulsion method. *Biophys. J.* **2014**, *107* (2), 346−354.

https://doi.org/10.1021/jacsau.4c00237
JACS Au 2024, 4, 2041−2049